Long-Term High-Speed Train–Track Dynamic Interaction Analysis Using a Moving Train–Track Interaction Model

Yan Xu[1], Caijin Yang[1](✉), Zhendong Liu[2], Weihua Zhang[1], and Sebastian Stichel[2]

[1] State Key Laboratory of Traction Power, Southwest Jiaotong University, Chengdu 610031, China
YangCJ@swjtu.edu.cn

[2] Department of Engineering Mechanics, KTH Royal Institute of Technology, Stockholm, Sweden

Abstract. A new moving train–track interaction model is shown in the paper to accurately and efficiently determine long-term high-speed train–track interaction dynamic response. In this model, the rail is represented with a reduced beam model (RBM) and the slabs mainly affected by the train–track interaction are modeled with four-node Kirchhoff-Love plate elements. The fastenings are modeled with spring-damper elements and the Concrete Asphalt (CA) layer is modeled with a Winkler foundation. Since only a small part of the rail and a few slabs from the whole slab track are included, the present model has fewer degrees of freedom than the traditional model using the modal superposition method and the simulation time is significantly decreased. The present model is validated by a long-term train–track interaction case where the results are compared with those from the traditional method. The simulation results show that the present model is accurate and efficient and has great advantages in solving high-speed train–track interaction problems.

Keywords: Train–track interaction · Reduced beam model · Slab track

1 Introduction

Train–track interaction plays an important role in high-speed railway engineering. The numerical study of the train–track interaction can directly reflect the dynamic characteristics of the train–track interaction and help researchers and engineers to better design and optimize the high-speed railway system [1], which has widely be used by researchers. With the increase in operational speed and the complex operation environment of the high-speed railway system, the train–track interaction system becomes more complex, and its modeling should better reflect different complex situations.

In the past decades, finite element method (FEM) and modal superposition method (MSM) have mainly been used in modeling the train–track interaction. Xiao et al. [2] investigated the effects of a failed ballasted track support on derailment behavior, in which a complex train-ballasted track interaction model was built up using the MSM,

A. Orlova and D. Cole (Eds.): IAVSD 2021, LNME, pp. 272–281, 2022.
https://doi.org/10.1007/978-3-031-07305-2_28

and the track support failure is modeled with zero stiffness and damping of the rail pad, fastening and ballast. Zhai et al. [3] developed a train-slab track interaction model using the MSM for the vehicle–track dynamic analysis, where this model was validated using experimental data. Torstensson et al. [4] modeled the wheelset–track interaction through the FEM to investigate the wheelset–track dynamic interaction ranging from 20 Hz to 2.5 kHz. Varandas et al. [5] studied the long-term deformation of the ballast and sub-ballast in the train–track interaction process, where the FEM was used to comprehensively model the track structure. However, when considering the long term train interaction with slab track, the flexibility of the slab must be considered, so both the FEM and MSM need to include a large number of degrees of freedom (DOFs) to model the whole structure of the slab track, especially when the track model is long. Therefore, the efficiency of the FEM and MSM in calculation is low.

In this work, a new moving train–track interaction model is developed to model the long-term train–track interaction in an accurate and efficient way. The slab track is studied, and a reduced beam model (RBM) [6] is used. The long slab track does not needed to be entirely modeled and only a small rail section around the train is considered and modeled using the RBM. With RBM used, only the slabs affected by the train–track interaction need to be modeled and the slab is modeled using Kirchhoff-Love plate elements. The fastenings are modeled as spring-damper elements and the CA mortar is modeled as Winkler foundation. Since only a small part of the slab track needs to be modeled, the number of DOFs of the train–track interaction model is reduced and the corresponding efficiency in calculation gets improved. The validation of the present model is checked against the traditional model by Zhai [3] that has been validated in the past.

The present moving train–track interaction model is described in Sect. 2 and the validation of the present model is shown in Sect. 3. Conclusions from the study are drawn in Sect. 4.

2 Formulation of the Moving Train–Track Interaction Model

Based on the theory of RBM, the moving train-slab track interaction model is formulated as shown in Fig. 1. As mentioned in [6], the vibration of the rail mainly concentrates on a small area around the train and dissipates significantly at the places far from the train due to damping effects, so with RBM only the affected part of the rail needs to be modeled. Moreover, in the slab track, the damping effect also exists in the CA mortar, so the vibration of the slab structure caused by the train–track interaction also mainly affects the slabs close to the train. Therefore, only the slabs affected by the train–track interaction need to be modeled, where the number of affected slabs is determined by the length of the RBM and slab.

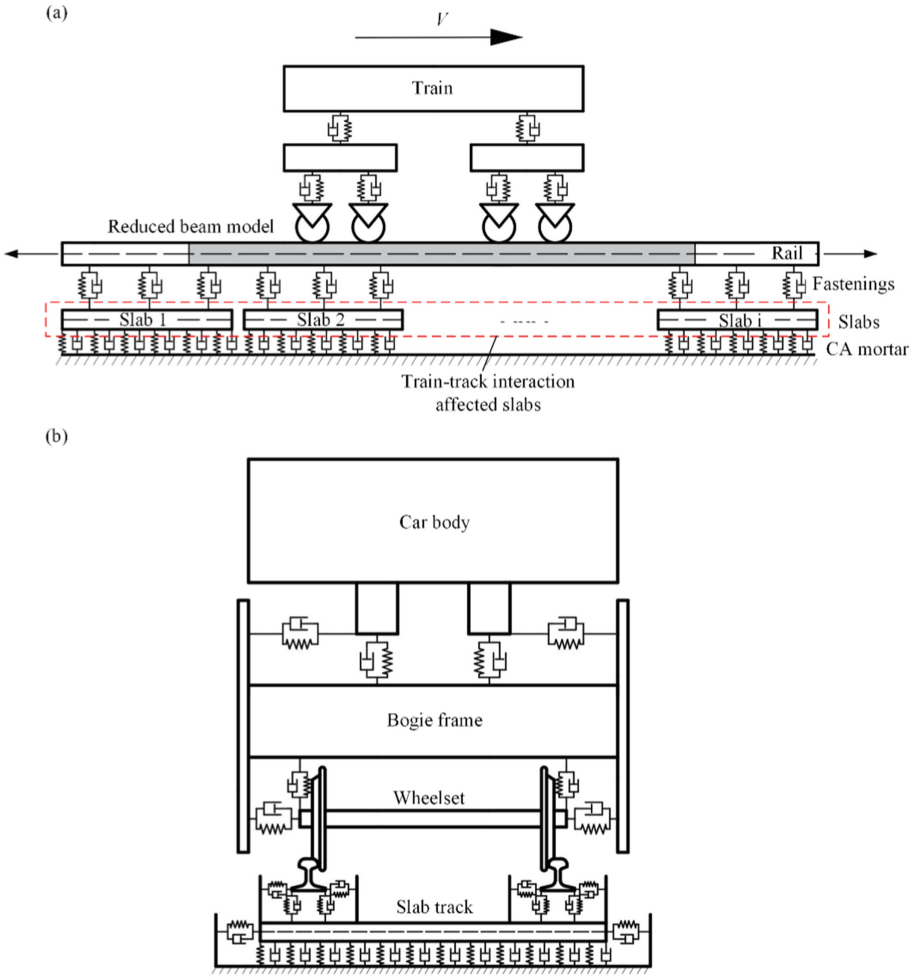

Fig. 1. Schematic of the moving train–track interaction model: (a) main view and (b) side view.

2.1 Model of the Slab Track

2.1.1 Model of the Rail

In the present model, the rail is considered as a Timoshenko beam and modeled using the RBM. With the length l of the RBM, the kinematic energy can be expressed as

$$T_r = \frac{1}{2}\int_0^l \rho A\dot{v}^2 ds + \frac{1}{2}\int_0^l \rho A\dot{w}^2 ds + \frac{1}{2}\int_0^l \rho\left(I_y + I_z\right)\dot{\theta}_x^2 ds + \frac{1}{2}\int_0^l \rho I_y\dot{\theta}_y^2 ds + \frac{1}{2}\int_0^l \rho I_z\dot{\theta}_z^2 ds \tag{1}$$

where ρ is the density of the rail, A is the area of the rail cross-section, and I_y and I_z are the second moments of the rail cross-section about y- and z-axes on the rail cross-section

reference coordinate system *o*-*xyz* [6], respectively. v and w are displacements of the cross-section central point o along the y- and z- axes, and θ_x, θ_y, and θ_z are rotation angles of the beam cross-section with respect to the x-, y-, and z-axes, respectively. The overdot denotes the time derivative. Similarly, the strain energy of the RBM is expressed in terms of beam coordinates v, w, θ_x, θ_y, and θ_z as

$$U_r = \frac{1}{2}\int_0^l \begin{pmatrix} EI_z\theta_z'^2 + EI_y\theta_z'^2 + GI_p\theta_z'^2 + k_{sz}GA\left(v' - \theta_z\right)^2 \\ +k_{sy}GA\left(w' - \theta_y\right)^2 \end{pmatrix} ds \tag{2}$$

where the operator $(\cdot)'$ denotes the partial derivative of a variable $(\cdot)$ with respect to coordinate x, E is the Young's modulus of the rail, G is the shear modulus of the rail, GI_p is the torsional stiffness of the rail, and k_{sy} and k_{sz} are shear coefficients along the y- and z-axes, respectively. Through using the Galerkin method, the displacements and rotations of the RBM are expressed as follows

$$v(x,t) = \mathbf{V}(x)\mathbf{q}_y(t),\, w(x,t) = \mathbf{W}(x)\mathbf{q}_z(t) \tag{3}$$

$$\theta_x(x,t) = \boldsymbol{\Phi}(x)\mathbf{q}_{\theta x}(t),\ \theta_y(x,t) = \boldsymbol{\Psi}_y(x)\mathbf{q}_{\theta y}(t),\, \theta_z(x,t) = \boldsymbol{\Psi}_z(x)\mathbf{q}_{\theta z}(t) \tag{4}$$

where $\mathbf{V}$, $\mathbf{W}$, $\boldsymbol{\Phi}$, $\boldsymbol{\Psi}_y$, and $\boldsymbol{\Psi}_z$ are trial functions, and $\mathbf{q}_y$, $\mathbf{q}_z$, $\mathbf{q}_{\theta x}$, $\mathbf{q}_{\theta y}$, and $\mathbf{q}_{\theta z}$ are the vectors of the corresponding generalized coordinates. The expressions of the above trial functions can be seen in [7].

Based on the theory of the RBM [6], in Eqs. (1) and (2), there are

$$\dot{v} = -V(t)\mathbf{V}'q_y + \mathbf{V}\dot{q}_y,\, \dot{w} = -V(t)\mathbf{W}'q_z + \mathbf{W}\dot{q}_z \tag{5}$$

$$\dot{\theta}_x = -V(t)\Phi' q_{\theta x} + \Phi\dot{q}_{\theta x},\, \dot{\theta}_y = -V(t)\Psi_y'\mathbf{q}_{\theta y} + \Psi_y\dot{\mathbf{q}}_{\theta y},\, \dot{\theta}_z = -V(t)\Psi_z'\mathbf{q}_{\theta z} + \Psi_z\dot{\mathbf{q}}_{\theta z} \tag{6}$$

$$v' = \mathbf{V}'q_y,\, w' = \mathbf{W}'q_y \tag{7}$$

$$\theta_x' = \Phi' q_{\theta x},\, \theta_y' = \Psi_y'\mathbf{q}_{\theta y},\, \theta_z' = \Psi_z'\mathbf{q}_{\theta z} \tag{8}$$

where $V(t)$ is the train velocity. Substituting Eqs. (10)–(13) into Eqs. (1) and (2) and using the Lagrange's equation, the dynamic equations of the rail can be written as

$$\mathbf{M}_r\ddot{\mathbf{q}}_r + \mathbf{C}_r\dot{\boldsymbol{q}}_r + \mathbf{K}_r\mathbf{q}_r = \mathbf{Q}_{flow} + \mathbf{Q}_{fr} \tag{9}$$

where the $\mathbf{M}_r$ is the mass matrix, $\mathbf{C}_r$ is the mass matrix, $\mathbf{K}_r$ is the stiffness matrix, and $\mathbf{q}_r = \left[\mathbf{q}_y,\ \mathbf{q}_z,\ \mathbf{q}_{\theta x},\ \mathbf{q}_{\theta y},\ \mathbf{q}_{\theta z}\right]^T$. $\mathbf{Q}_{fr}$ is the generalized force vector of wheel–rail interaction forces and fastening forces applied to the rails, and $\mathbf{Q}_{flow}$ is the additional generalized force vector. A detailed derivation and expressions of the above matrices and generalized forces in Eq. (14) can be found in [6].

2.1.2 Model of the Slab

In most of the slab tracks like CRTS II, the slab is much longer than it is thick (thickness to width and length ratio less than 0.1) [8]. Therefore, the slab is considered as a thin plate structure and modeled using the Kirchhoff-Love plate theory and FEM. Since the bending stiffness of the slab in the lateral direction is much higher than in the vertical direction [8], only the vertical deformation of the plate is considered, and the slab is regarded as a rigid body when considering its lateral motion. The kinematic energy of the plate element can be expressed as

$$T_P = \frac{1}{24}\rho_P h^3 \iint_S \left(\dot{w}_{Px}^2 + \dot{w}_{Py}^2\right) dxdy + \frac{1}{2}\rho_P h \iint_S \dot{w}_P^2 dxdy \tag{10}$$

where w_P is the vertical displacement of the plate element, w_{Px} and w_{Py} denote the partial derivate of w_P with respect to coordinates x_P and y_P of the plate element, respectively. h is the thickness of the plate, ρ_P is the density of the plate, and S indicates the middle surface of the plate element. The strain energy of the plate element is

$$U_P = \frac{1}{2}\iint_\Omega \boldsymbol{\kappa}^T \mathbf{D}\boldsymbol{\kappa} dxdy \tag{11}$$

where $\boldsymbol{\kappa}^T = \left[\kappa_x \ \kappa_y \ \kappa_{xy}\right]$ is the generalized strain vector of the plate element, $\mathbf{D}$ is the elasticity matrix. In the vector $\boldsymbol{\kappa}$, there are

$$\kappa_x = -\frac{\partial^2 w_P}{\partial x_P^2},\ \kappa_y = -\frac{\partial^2 w_P}{\partial y_P^2},\ \kappa_{xy} = -2\frac{\partial^2 w_P}{\partial x_P \partial y_P} \tag{12}$$

$$\mathbf{D} = D_0 \begin{bmatrix} 1 & \nu & 0 \\ \nu & 1 & 0 \\ 0 & 0 & \frac{1-\nu}{2} \end{bmatrix} \tag{13}$$

In Eq. (18), D_0 is the rigidity of the plate, and ν is the Poisson's ratio. Based on the finite element theory, the vertical displacement of the plate element can be expressed as

$$w_P = \mathbf{N}_P \mathbf{q}_P \tag{14}$$

where $\mathbf{N}_P$ is the shape function vector of the plate element and $\mathbf{q}_P$ is the generalized coordinate vector of the plate element. Detailed expressions of $\mathbf{N}_P$ and $\mathbf{q}_P$ are shown in [9]. Based on Eqs. (15) and (16) and applying Lagrange's equation, the dynamic matrix equation of the plate element becomes

$$\mathbf{M}_P \ddot{\mathbf{q}}_P + \mathbf{C}_P \dot{\boldsymbol{q}}_P + \mathbf{K}_P \mathbf{q}_P = \mathbf{Q}_{fP} \tag{15}$$

where $\mathbf{M}_P$ is the mass matrix, $\mathbf{C}_P$ is the mass matrix, $\mathbf{K}_P$ is the stiffness matrix, and $\mathbf{Q}_{fP}$ is the generalized force vector of fastening forces and CA mortar forces applied to the plate element in vertical direction. Detailed derivations of these matrices and the force vector can be seen in Ref. [10].

The dynamic equations of the whole slab structure are then derived. Since only the train–track interaction affected slabs need to be modeled, the number of these slabs is

calculated before modeling the slab structure. The number of train–track interaction affected slabs n_{sf} can also be determined through the equation

$$n_{sf} = floor\left(\frac{l}{l_S + l_G}\right) + 1 \tag{16}$$

where the floor means the round down of the closest real number, l_S is the length of the slab, and l_G is the width of the gap between every slab.

Based on the number of affected slabs, the dynamic equation of the slab structure in the present model is

$$\mathbf{M}_{SA}\ddot{\mathbf{q}}_{SA} + \mathbf{C}_{SA}\dot{\boldsymbol{q}}_{SA} + \mathbf{K}_{SA}\mathbf{q}_{SA} = \mathbf{Q}_{fSA} \tag{17}$$

where

$$\mathbf{M}_{SA} = \begin{bmatrix} \mathbf{M}_S & & & \\ & \mathbf{M}_S & & \\ & & \ddots & \\ & & & \mathbf{M}_S \end{bmatrix}_{n_{sf}\times n_{sf}}, \quad \mathbf{C}_{SA} = \begin{bmatrix} \mathbf{C}_S & & & \\ & \mathbf{C}_S & & \\ & & \ddots & \\ & & & \mathbf{C}_S \end{bmatrix}_{n_{sf}\times n_{sf}} \tag{18}$$

$$\mathbf{K}_{SA} = \begin{bmatrix} \mathbf{K}_S & & & \\ & \mathbf{K}_S & & \\ & & \ddots & \\ & & & \mathbf{K}_S \end{bmatrix}_{n_{sf}\times n_{sf}} \tag{19}$$

$\mathbf{M}_S$, $\mathbf{C}_S$, and $\mathbf{K}_S$ are the mass matrix, stiffness matrix and damping matrix of one single slab, respectively, based on Eq. (20) and finite element theory [11]. $\mathbf{Q}_{fSA}$ is the generalized force vector of fastening forces and CA mortar forces applied to the slab structure in the vertical direction. Its derivation progress is the same as those shown in [11]. The corresponding generalized coordinate vector $\mathbf{q}_{SA}$ is expressed as

$$\mathbf{q}_{SA} = \left[\mathbf{q}_S,\ \mathbf{q}_S,\ \cdots,\ \mathbf{q}_S\right]^T \tag{20}$$

where $\mathbf{q}_S$ is the generalized coordinate vector of one single slab developed by $\mathbf{q}_P$. Its detailed derivation progress is shown in [11].

The fastenings and CA mortars are finally considered here. The fastening is modeled as spring-damping element and the CA mortar is modeled as Winkler foundation [3]. Note that the location of the fastenings in the relative coordinate system of the moving train–track interaction model changes with time and should be calculated at every time step [6].

2.2 Model of the Train–Track Interaction

With the dynamic equations of the slab track, the train–track interaction model is obtained here. In the train–track interaction, the vehicle model is just the same as those shown in [6]. The normal wheel–rail contact forces are calculated through Hertz's formulae [11]

and creep forces are calculated according to the heuristic formulae of Shen et al. [12]. The normal and creep forces act on both the wheelsets and the rail.

The whole dynamic equations of the moving train–track interaction system are shown as

$$\begin{bmatrix} \mathbf{M}_{rl} & & & \\ & \mathbf{M}_{rr} & & \\ & & \mathbf{M}_{SA} & \\ & & & \mathbf{M}_{v} \end{bmatrix} \begin{bmatrix} \ddot{\mathbf{q}}_{rl} \\ \ddot{\mathbf{q}}_{rr} \\ \ddot{\mathbf{q}}_{SA} \\ \ddot{\mathbf{q}}_{v} \end{bmatrix} + \begin{bmatrix} \mathbf{C}_{rl} & & & \\ & \mathbf{C}_{rr} & & \\ & & \mathbf{C}_{SA} & \\ & & & \mathbf{C}_{v} \end{bmatrix} \begin{bmatrix} \dot{\boldsymbol{q}}_{rl} \\ \dot{\boldsymbol{q}}_{rr} \\ \dot{\boldsymbol{q}}_{SA} \\ \dot{\boldsymbol{q}}_{v} \end{bmatrix} + \begin{bmatrix} \mathbf{K}_{rl} & & & \\ & \mathbf{K}_{rr} & & \\ & & \mathbf{K}_{SA} & \\ & & & \mathbf{K}_{v} \end{bmatrix} \begin{bmatrix} \mathbf{q}_{rl} \\ \mathbf{q}_{rr} \\ \mathbf{q}_{SA} \\ \mathbf{q}_{v} \end{bmatrix} = \begin{bmatrix} \mathbf{Q}_{rl} \\ \mathbf{Q}_{rr} \\ \mathbf{Q}_{SA} \\ \mathbf{Q}_{v} \end{bmatrix} \tag{21}$$

where $\mathbf{M}_{rl}$ and $\mathbf{M}_{rr}$ are the mass matrices of the rail at left and right side, $\mathbf{C}_{rl}$ and $\mathbf{C}_{rr}$ are the damping matrices of the rail on the left and right side, and $\mathbf{K}_{rl}$ and $\mathbf{K}_{rr}$ are the stiffness matrices of the rail on the left and right side. $\mathbf{Q}_{rl}$ and $\mathbf{Q}_{rr}$ are the generalized force vectors of the wheel–rail contact forces and fastenings on the rail on the left and right sides. $\mathbf{M}_{v}$, $\mathbf{C}_{v}$, and $\mathbf{K}_{v}$ are the mass, damping and stiffness matrices of the vehicle, respectively.

After modeling the train–track interaction, the present model is implemented in MATLAB and its dynamic equations are solved using the MATLAB function ode15s. The initial condition of the generalized coordinate array is zero. The track irregularity is generated based on the power spectral density of a German high-speed track spectrum with low irregularity shown in [6]. This power spectral density of the track is used as input excitation in the computational process of the wheel–rail normal contact force.

3 Results and Discussion

To validate the accuracy of the present model, a long-term train–track interaction case is considered in this part. Parameters of the slab track can be seen in [13]. The train moves with a constant speed $V = 350$ km/h and the track length is 600 m. The dynamic responses of the train–track interaction obtained are compared with those from the traditional model developed by Zhai et al. [3], which was validated by measurement data and used by many researchers. In this traditional model, the MSM is used to model the rail and slabs. The fastenings and CA mortar are modeled as spring-damping element and Winkler foundations, respectively. The whole 600 m track is modeled in the traditional model, but only 36 m rail and 7 slabs are considered in the present model. In the traditional model, the first 1200 modes of the rails are considered, and the first 20 modes of the slab are considered. There are 16427 DOFs in the traditional model. In the present model, the first 60 modes of the RBM are considered and 18 elements are used in the modeling of a single slab. There are 943 DOFs in the present model. The vehicle model mentioned above is also used in the traditional model. Both the present model and the traditional model are solved using the MATLAB function ode15s with the same time step and time of the train–track interaction.

The vertical and lateral wheel–rail contact forces are used in the study to validate the accuracy of the present model. Time histories of the vertical wheel–rail contact forces of Wheelset 1 left and right wheel are shown in Fig. 2, and lateral wheel–rail contact forces of Wheelset 1 left and right wheel are shown in Fig. 3. The results in Figs. 2 and 3 show that the present model has a good agreement with the traditional model that is validated against measurements. As shown in these figures, the maximum relative difference between these two models in calculating the dynamic response of the train–track interaction is small. The maximum relative difference between the two models is 3.8% and shown by the results of the lateral wheel–rail contact force in Fig. 2(c) and (d). We can conclude that the present model is accurate in solving train-slab track interaction dynamics.

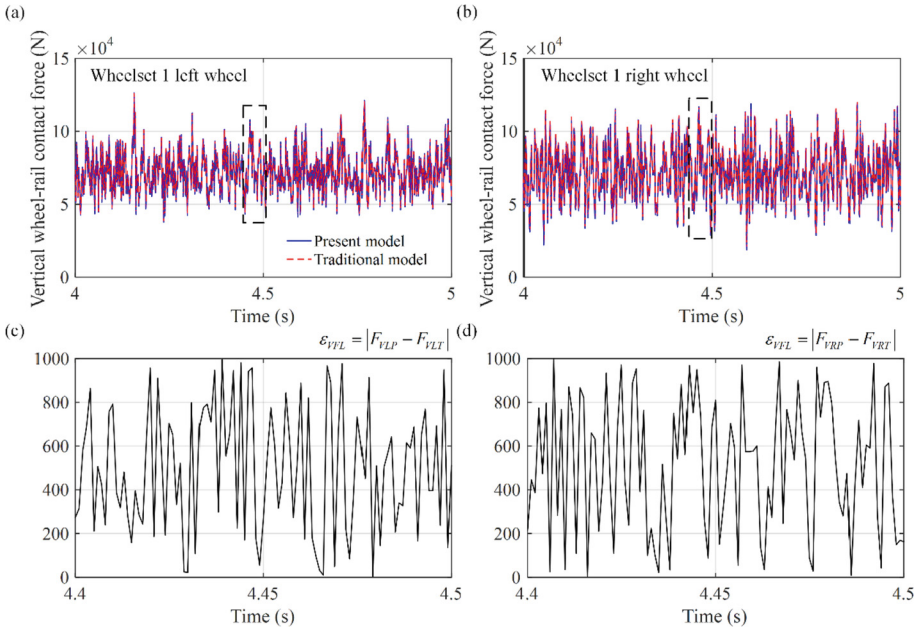

Fig. 2. Time histories of the vertical wheel–rail contact force of Wheelset 1 from the present model and the traditional model: (a) vertical wheel–rail contact force of left wheel; (b) vertical wheel–rail contact force of right wheel; (c) absolute difference of the vertical wheel–rail contact force of left wheel between the present model F_{VLP} and the traditional model F_{VLT} and (d) absolute difference of the vertical wheel–rail contact force of left wheel between the present model F_{VRP} and the traditional model F_{VRT}.

The present model has a higher computational efficiency than the traditional model, because there are 16427 DOFs in the traditional model but only 943 DOFs in the present model. Based on this, the calculation time of the present model for the validation case is 42261s and 88532s for the traditional model. The calculations are carried out on the same computer with Intel Xeon W-2115 and 32 GB DDR4 RAM. We can conclude that

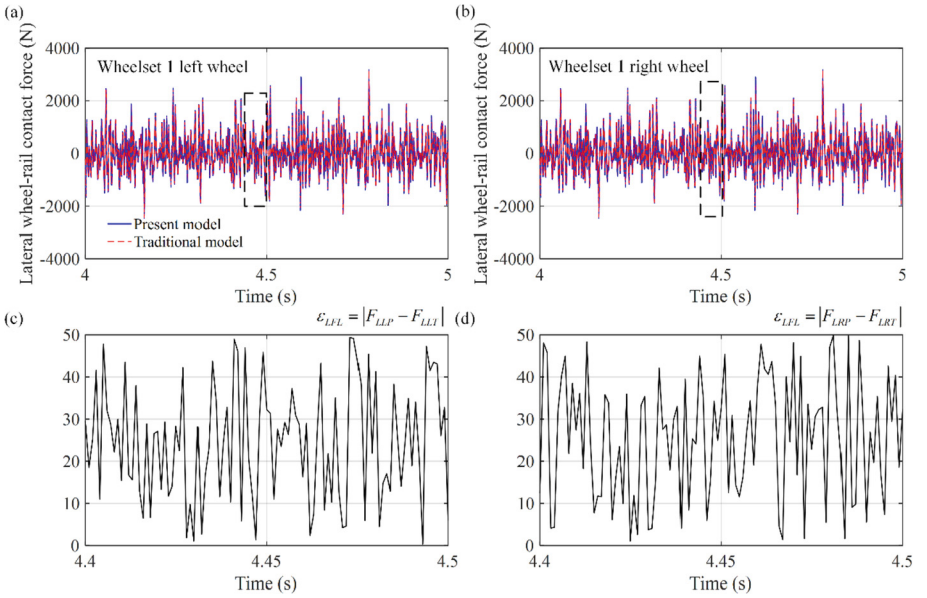

Fig. 3. Time histories of the lateral wheel–rail contact force of Wheelset 1 left and right wheel from the present model and traditional model: (a) lateral wheel–rail contact force of left wheel; (b) lateral wheel–rail contact force of right wheel; (c) absolute difference of the lateral wheel–rail contact force of left wheel between the present model F_{LLP} and the traditional model F_{LLT} and (d) absolute difference of the lateral wheel–rail contact force of right wheel between the present model F_{LRP} and the traditional model F_{LRT}.

the present model has a big advantage of reducing calculation time in studying long-term train–track interaction dynamics.

4 Conclusion

In this paper, a new moving train–track interaction model is developed to calculate the dynamic responses of long-term high-speed train–track interaction. In the model, only a small part of the track around the train instead of the whole track need to be modeled based on the theory of the reduced beam model (RBM). The reduced rail is modeled using the RBM, and these slabs are modeled using Kirchhoff-Love plate elements. Since only a small number of slabs instead of all the slabs need to be modeled, the number of DOFs is significantly reduced when comparing with traditional models based on the modal superposition method (MSM) and the calculation time is therefore reduced. The present model is checked against Zhai's model, where a high-speed train–track interaction model is considered. Based on the obtained calculation results, the present model is calculating the train–track interaction dynamics with the same accuracy as the traditional model but with much shorter calculation times, which makes it an efficient tool in investigating the influence of fastening failure on train–track interaction dynamics.

Acknowledgements. The authors would like to thank supports from the National Natural Science Foundation of China (Grant no. 12072293), the Project of State Key Laboratory of Traction Power for Southwest Jiaotong University (Grant no. 2021TPL-T 10), China Scholarship Council (Grant no. 202007000115), and the Open Project funded by the State Key Laboratory of Traction Power, Southwest Jiaotong University (Grant no. TPL2004).

References

1. Cai, X.P., Luo, B.C., Zhong, Y.L., et al.: Arching mechanism of the slab joints in CRTSII slab track under high temperature conditions. Eng. Fail. Anal. **98**, 95–108 (2019)
2. Xiao, X., Jin, X., Deng, Y., et al.: Effect of curved track support failure on vehicle derailment. Veh. Syst. Dyn. **46**, 1029–1059 (2008)
3. Zhai, W., Wang, K., Cai, C.: Fundamentals of vehicle–track coupled dynamics. Veh. Syst. Dyn. **47**, 1349–1376 (2009)
4. Torstensson, P.T., Nielsen, J.C.O., Baeza, L.: Dynamic train–track interaction at high vehicle speeds—Modelling of wheelset dynamics and wheel rotation. J. Sound Vib. **330**, 5309–5321 (2011)
5. Varandas, J.N., Paixão, A., Fortunato, E., et al.: Long-term deformation of railway tracks considering train–track interaction and non-linear resilient behaviour of aggregates—a 3D FEM implementation. Comput. Geotech. **126**, 103712 (2020)
6. Yang, C.J., Xu, Y., Zhu, W.D., et al.: A three-dimensional modal theory-based Timoshenko finite length beam model for train–track dynamic analysis. J. Sound Vib. **479**, 1–22 (2020)
7. Zhang, W., Shen, Z., Zeng, J.: Study on dynamics of coupled systems in high-speed trains. Veh. Syst. Dyn. **51**, 966–1016 (2013)
8. Aggestam, E., Nielsen, J.C.O.: Simulation of vertical dynamic vehicle–track interaction using a three-dimensional slab track model. Eng. Struct. **222**, 110972 (2020)
9. Wu, J.-S, Lee, M.-L., Lai, T.-S.: The dynamic analysis of a flat plate under a moving load by the finite element method. Int. J. Numer. Methods Eng. 24, 743–762 (1987)
10. Mats, G.L., Bengzon, F.: The Finite Element Method: Theory, Implementation, and Applications, Springer, Heidelberg, New York, Dordrecht, London (2011)
11. Xiao, X., Jin, X., Wen, Z., et al.: Effect of tangent track buckle on vehicle derailment. Multibody Syst. Dyn. **25**, 1–41 (2011)
12. Shen, Z.Y., Hedrick, J.K., Elkins, J.A.: Comparison of alternative creep force models for rail vehicle dynamic analysis. Dynamics of Vehicles on Roads and Tracks: Proceedings of the IAVSD Symposium of International Association, pp. 591–605 (1984)
13. Zeng, Z., Liu, F., Lou, P., et al.: Formulation of three-dimensional equations of motion for train—slab track—bridge interaction system and its application to random vibration analysis. Appl. Math. Model. **40**, 5891–5929 (2016)